Bioactive Materials 12 (2022) 1–15

Contents lists available at ScienceDirect

Bioactive Materials

journal homepage: www.keaipublishing.com/en/journals/bioactive-materials

Osteogenic and anti-tumor Cu and Mn-doped borosilicate nanoparticles for syncretic bone repair and chemodynamic therapy in bone tumor treatment

Libin Pang [a,c,1], Renliang Zhao [b,1], Jing Chen [d,1], Jingxin Ding [a], Xiaochen Chen [a], Wenwen Chai [a], Xu Cui [c], Xiaolin Li [b,**], Deping Wang [a,*], Haobo Pan [c,***]

[a] School of Materials Science and Engineering, Tongji University, Shanghai, 201804, China
[b] Department of Orthopedic Surgery, and Shanghai Institute of Microsurgery on Extremities, Shanghai Jiao Tong University Affiliated Sixth People's Hospital, Shanghai, 200233, China
[c] Shenzhen Institutes of Advanced Technology, Chinese Academy of Sciences, Shenzhen, 518055, China
[d] Shuguang Hospital Affiliated to Shanghai University of Traditional Chinese Medicine, Shanghai, 201203, China

ARTICLE INFO

Keywords:
Borosilicate
Bio-ceramics
Bone regeneration
Tumor therapy
Chemodynamic therapy
Bone tumor treatment

ABSTRACT

Critical bone defects caused by extensive excision of malignant bone tumor and the probability of tumor recurrence due to residual tumor cells make malignant bone tumor treatment a major clinical challenge. The present therapeutic strategy concentrates on implanting bone substitutes for defect filling but suffers from failures in both enhancing bone regeneration and inhibiting the growth of tumor cells. Herein, Cu and Mn-doped borosilicate nanoparticles (BSNs) were developed for syncretic bone repairing and anti-tumor treatment, which can enhance bone regeneration through the osteogenic effects of Cu^{2+} and Mn^{3+} ions and meanwhile induce tumor cells apoptosis through the hydroxyl radicals produced by the Fenton-like reactions of Cu^{2+} and Mn^{3+} ions. *In vitro* study showed that both osteogenic differentiation of BMSCs and angiogenesis of endothelial cells were promoted by BSNs, and consistently the critical bone defects of rats were efficiently repaired by BSNs through *in vivo* evaluation. Meanwhile, BSNs could generate hydroxyl radicals through Fenton-like reactions in the simulated tumor microenvironment, promote the generation of intracellular reactive oxygen species, and eventually induce tumor cell apoptosis. Besides, subcutaneous tumors of mice were effectively inhibited by BSNs without causing toxic side effects to normal tissues and organs. Altogether, Cu and Mn-doped BSNs developed in this work performed dual functions of enhancing osteogenesis and angiogenesis for bone regeneration, and inhibiting tumor growth for chemodynamic therapy, thus holding a great potential for syncretic bone repairing and anti-tumor therapy.

1. Introduction

Malignant bone tumor, commonly known as an aggressive and unpredictable disease that tends to recrudesce, should be treated with surgical resection to avoid tissue infiltration and malignancy according to the latest Guidelines of National Comprehensive Cancer Network (NCCN) [1]. Treatment aims to prevent damage to the bone near the affected joint, but extensive excision of tumor will leave critical bone defects difficult to be repaired [2]. Generally, autogenous or allogenic bones are loaded to expectedly restore the function of bone, but unfortunately they are lack of resources or in risk of immune rejection [3]. Moreover, the residual tumor cells that are not fully removed raise the risk of tumor recurrence [4].

Artificial bone substitutes are generally reported to repair bone defects by inducing bone growth [5–7]. However, bone substitutes currently in clinical use still lack sufficient bioactivity to enhance bone regeneration [8]. Moreover, the lack of anti-tumor function makes such substitutes incapable of killing tumor cells which may remain after

Peer review under responsibility of KeAi Communications Co., Ltd.
* Corresponding author.
** Corresponding author.
*** Corresponding author.
E-mail addresses: lixiaolin@sjtu.edu.cn (X. Li), wdpshk@tongji.edu.cn (D. Wang), hb.pan@siat.ac.cn (H. Pan).
[1] These authors contributed equally to this work.

https://doi.org/10.1016/j.bioactmat.2021.10.030
Received 25 June 2021; Received in revised form 23 September 2021; Accepted 19 October 2021
Available online 25 October 2021

clinical surgery, and thus the chance of activation and metastasis of tumor cells rises [9–11]. Therefore, there is an urgent need for an artificial highly bioactive bone substitute that achieved syncretic bone regeneration and tumor therapy for bone tumor treatment [9].

A new group of bio-ceramics, named borosilicate (BS), with the dual network of interconnected [SiO_4] and [BO_3], is showing potential to spontaneously regulate the osteogenesis of stem cells and promote bone regeneration. The advantages of such composition lie in the controllable degradation with the adjustment of [SiO_4]/[BO_3] ratio, and in the meantime a number of ions can be incorporated to fulfill the different biological functions [12–15]. We have previously reported the anticipated bone regeneration could be attributed to the synergic effects both by the increase of pH and functional ions such as Si, B and Ca, since the alkaline microenvironment was beneficial to spontaneously balance the activity of osteoblasts and osteoclasts, that is, enhancing the activity of osteoblasts and meanwhile inhibiting the activity of osteoclasts [16]. Besides, the biological functions of Si, B and Ca ions were widely reported to stimulate new bone formation [12–15]. Therefore, we postulate the acceleration of new bone formation can be achieved both by pH effects and functional ions of borosilicate.

Although borosilicate shows great potential in bone repairing as highly bioactive material, the current developed borosilicate didn't take into account the needs for anti-tumor treatment, which cannot achieve osteogenesis and anti-tumor therapy simultaneously [9–11]. In response to this issue, researchers have synthesized mesoporous bio-ceramics that can be loaded with drugs, adopting drug-loaded bio-ceramics for anti-tumor treatment [17]. Meanwhile, composites of bio-ceramics and other functional materials, such as photothermal materials were also developed for anti-tumor treatment like photothermal therapy [18,19]. However, such studies are often based on complex structure designs, with high application thresholds. Few studies have tried to achieve the anti-tumor function of the bio-ceramic itself. Here, we attempt to design a new borosilicate composition to endow borosilicate anti-tumor function.

Cu^{2+} and Mn^{3+} ions have been found to undergo Fenton or Fenton-like reactions in an acidic environment with high content of hydrogen peroxide (H_2O_2) to produce hydroxyl radicals (·OH) with high oxidizing properties [20]. And it's also found that tumor microenvironment is featured by slight acidity and overexpression of both hydrogen peroxide and glutathione [21]. Therefore, Cu^{2+} and Mn^{3+} ions are supposed to generate high oxidizing hydroxyl radicals in the tumor microenvironment and trigger tumor cell apoptosis. According to this principle, chemodynamic therapy (CDT) has been developed for anti-tumor treatment [22–26]. Inspired by this, it's hypothesized that incorporating Cu and Mn into the network of borosilicate may endow borosilicate the anti-tumor function. The resulting Cu or Mn doped borosilicate will gradually degrade and release ions into the tumor microenvironment, producing hydroxyl radicals to induce tumor cell apoptosis. And the released Cu^{2+} and Mn^{3+} ions will also be capable of promoting osteogenic differentiation of bone marrow stromal cells (BMSCs) to enhance the osteogenic capacity of borosilicate according to previous studies [27,28]. Therefore, borosilicate incorporated with Cu or Mn which can steadily release Cu^{2+} and Mn^{3+} ions are expected to achieve the dual functions of promoting bone formation and anti-tumor treatment through chemodynamic therapy.

Furthermore, to improve the activity of borosilicate materials and increase the tissue penetration of borosilicate, Cu and Mn doped borosilicate nanoparticles (BSNs) were synthesized through sol-gel soft template method [29]. To validate the bifunctionality of the prepared BSNs, firstly, the physicochemical properties of BSNs were characterized, and the effects of BSNs on the proliferation and osteogenic differentiation of BMSCs and migration and tube formation of endothelial cells *in vitro* were investigated. Then the repairing of rat femoral defects and angiogenesis *in vivo* were evaluated. Meanwhile, to verify the anti-tumor performance of BSNs, the production of hydroxyl radicals in simulated tumor environment was determined, and the inhibition of BSNs on tumor cells *in vitro* as well as the production of intercellular ROS were examined. And then anti-tumor effects of BSNs on mouse subcutaneous tumors were assessed. Finally, the potential of BSNs designed in this work being used for syncretic bone defect repairing and tumor therapy after bone tumor surgery was discussed.

2. Materials and method

2.1. Materials

Tetraethyl Orthosilicate (TEOS), Triethyl Phosphate (TEP), Tributyl Borate (TBB), Calcium Nitrate Tetrahydrate (CaN), Manganese (II) Nitrate Tetrahydrate (MnN), Copper Nitrate Trihydrate (CuN), Cetyltrimethylammonium Bromide (CTAB), Absolute Ethanol and Nitric Acid are all analytically pure reagents and bought from Shanghai aladdin Biochemical Technology Co., Ltd, and are used as received.

2.2. Preparation of borosilicate nanoparticles

Borosilicate nanoparticles (BSNs) were prepared using sol-gel soft template method modified from previous studies [30], and four types of bioactive borosilicate were synthesized, which were respectively the undoped borosilicate nanoparticles (BSNs), copper-doped borosilicate nanoparticles (BSNs-Cu), manganese-doped borosilicate nanoparticles (BSNs-Mn) and copper-manganese-co-doped borosilicate nanoparticles (BSNs-Cu-Mn). The specific method was as follows: 0.729g of CTAB and 3.3 ml of ammonia solution (25 wt%) were dissolved in 200 ml deionized water at 40 °C. After the solution was clear and uniform, a mixture of 2.6 ml of TEOS, 0.9 ml of TBB and 0.2 ml of TEP was added dropwise to the solution, and then magnetically stir vigorously. After 30 min of reaction, 0.6g of CaN aqueous solution (2 ml) was added dropwise. After that, 0.2g of CuN aqueous solution (1 ml), 0.2g of MnN aqueous solution (1 ml), and 0.2g of CuN and 0.2g of MnN aqueous solution (1 ml) were added respectively for the preparation of BSNs-Cu, BSNs-Mn and BSNs-Cu-Mn and stir for another 4h. Then the particles were centrifuged, rinsed with ethanol and deionize water several times, and freeze-dried for 48h, and finally sintered at 600 °C for 180min (heating rate 2 °C/min) to obtain borosilicate nanoparticles.

2.3. Characterization of BSNs

The composition of the four kinds of BSNs were determined by inductively coupled plasma optical emission spectroscopy (ICP-OES, PerkinElmer Optima 8300). In brief, 20 mg of BSNs were dissolved in 1 ml of HF solution, then the solution was diluted 500 times with deionized water. The concentration of Si, B, Ca, P, Mn and Cu in the solution was measured by ICP-OES, from which the composition of BSNs could be calculated. The structure of the prepared materials was characterized by X-ray diffraction (XRD, Rigaku D/max 2550), and Fourier transform infrared (FTIR, Bruker EQUINOXSS/HYPERION2000). At the same time, the morphology of the prepared BSNs was characterized by transmission electron microscopy (TEM, Joel JEM-2100F). The valence of copper and manganese incorporated into the borosilicate were analyzed by X-ray photoelectron spectroscopy (XPS, Thermo Fisher Scientific ESCALAB 250Xi). And the degradation and ion releasing of BSNs was determined by ICP-OES as follows: 20 mg of BSNs were soaked in 10 ml of PBS solution, then 5 ml of solution was taken out every two days for ICP-OES analysis to determine the concentration of various ions in the soaking solution, and 5 ml of fresh PBS was added back to the immersion solution. To study the mineralization of BSNs, BSNs powders were immersed in PBS solution at 37 °C for a period of time, and then BSNs were centrifuged and dried. The formation of apatite was examined by XRD, and the microscopic morphology of the apatite was observed by scanning electron microscope (SEM, FEI Quanta 200F).

2.4. Bone repairing evaluation

2.4.1. Proliferation and differentiation of BMSCs in vitro

Primary rBMSCs are extracted from the femur of 2-week-old S-D rats, and cultured in minimum essential medium α-MEM (α-MEM; Gibco) with 10% fetal bovine serum (FBS; Gibco), 1% penicillin (100 U/ml) and streptomycin (100 μg/ml) (Gibco) in an incubator with 5% CO_2 at 37 °C, and used for following experiments [31]:

To investigate the effect of BSNs on the proliferation of rBMSCs, Cell Counting Kit-8 assay (CCK-8; Dojindo, Japan) was performed. Before the assay, the cells were counted using a hemocytometer. In brief, 15–20 μl of cell suspension was added between the hemocytometer and cover glass. Then count the number of cells in all four outer squares divide by four (the mean number of cells/square). The number of cells per square $*10^4$ = the number of cells/ml of suspension. The original cell suspension was then diluted to the appropriate cell concentration and then added to each well of a 96-well plate to achieve a density of 1×10^3 cells/well (n = 6). After incubation for 1d, the medium was replaced with 100 μl of culture medium containing BSNs (50 μg/ml). At day 1, 3 and 7, the medium of each well was placed with 100 μl of fresh medium containing 10% CCK-8 solution. After incubation for 2 h, the light absorbances were measured at 450 nm with a microplate reader (BioRad 680, USA).

To determine the ALP activity of rBMSCs, 1×10^5 cells were seeded in a 24-well plate and co-cultured with BSNs (50 μg/ml) for 7 and 14 day (n = 3). At each time point, the culture medium was decanted, and each well was washed gently three times with PBS and once with 50 mM Tris buffer (0 °C), and the cells were lysed in 200 μl 0.2% Triton X-100. Then lysates were centrifuged at 14 000 rpm for 15 min at 4 °C 50 μl of the supernatant was mixed with 150 μl of the working solution according to the manufacturer's protocol (Beyotime Institute of Technology, Shanghai, China). The content of *p*-nitrophenol was determined by measuring the absorbance at 405 nm with a microplate reader (Bio-Rad 680, USA). The ALP activity was calculated from a standard curve after normalizing to the total protein content and the results were expressed in nanomoles of *p*-nitrophenol produced per minute per milligram of protein.

The expression of osteogenesis-related genes including BMP2, COL1A1 and RUNX2 were measured by the qRT-PCR analysis. Typically, rBMSCs were co-cultured with BSNs (50 μg/ml) for 3 and 7 days and harvested using Trizol (Invitrogen) to extract the RNA (n = 3). The obtained RNA was reverse transcribed into complementary DNA (cDNA) using reverse transcription kit (EZBioscience®, Shanghai, China) and the qRT-PCR was performed using SYBR green mix (EZBioscience® SYBR green master mix, Shanghai, China) and the amplification plots obtain from the light cycer® 480 system (Roche LC 480, Switzerland). The relative expression of the genes of interest was normalized against the housekeeping gene GAPDH.

To observe osteogenic differentiation of rBMSCs *in vitro* more clearly, ALP and alizarin red staining were conducted. On day 21, the rBMSCs co-cultured with BSNs (50 μg/ml) in the 24-well transwell plate were washed to a 24-well plate after trypsinization and fixed with 2.5% glutaraldehyde and washed twice with PBS, then stained with BCIP/NBT kit (Beyotime Biotechnology, China) and 1 mM alizarin red (Cyagen, USA) for 10 min individually. Photos were acquired with a microscope (Leica, Germany). The positive area (%) of ALP and ARS stainings were calculated by ImageJ software.

2.4.2. Proliferation, migration and tube formation of EaHy926 in vitro

The human umbilical vein cell line (EaHy926) was cultured in minimum essential high glucose DMEM (hDMEM, Gibco) with 10% fetal bovine serum (Gibco) in an incubator with 5% CO_2 at 37 °C, and used for following tests [32]. The proliferation of EaHy926 co-cultured with BSNs (50 μg/ml) was determined by CCK-8. The specific method was the same as the description in section 2.4.1.

To measure the migration potential of EaHy926, a transwell assay was conducted. Firstly, 5.0×10^4 cells/ml were seeded in the upper chambers of a 24-well transwell plate (3422, Corning) and 600 μl of culture medium containing BSNs (50 μg/ml) was added to the lower chambers (n = 3). After 24 h of incubation, the cells on the upper surface of the transwell membrane were gently wiped with a cotton swab, and cells on the lower surface were fixed with 4% paraformaldehyde and stained with 0.5% crystal violet for 10 min. Finally, six random lower surface areas of each filter were counted twice in a blinded manner by two independent evaluators.

Meanwhile, the tube formation ability of EaHy926 was tested by seeding the cells on Matrigel (BD Bioscience). In brief, 500 μl of cold Matrigel solution containing 50 μg/ml BSNs per well was spread in each well of a 24-well plate and left to gelatinize at 37 °C for 30 min, then a EaHy926 suspension containing 2.0×10^4 cells/ml cells were seeded on the matrix (n = 3). After 9 h of incubation, the number of complete capillaries connecting individual points of each well was counted to evaluate the tube formation ability.

Furthermore, the expression of VEGF was detected by an Elisa kit (Invitrogen). In brief, the cells were cultured with BSNs (50 μg/ml) at a density of 2.0×10^4 cells/ml in a 24-well plate. After 3 days of incubation, the cells were harvested and lysed in 200 μl 0.2% Triton X-100. Then lysates were centrifuged at 14 000 rpm for 15 min at 4 °C 200 μl of the supernatant was used for the quantitative detection of VEGF by Elisa kit. The results were normalized by the concentration of total protein for all samples and calculated from a standard curve.

2.4.3. The repairing of rat femoral defects in vivo

All animal surgical procedures were approved by the Animal Care and Experiment Committee of Shanghai Jiao Tong University Affiliated Sixth People's Hospital [31]. In brief, 25 adult S-D rats (8 weeks old; weight 250 ± 25 g) were anaesthetized by intraperitoneal injection of 4% chloral hydrate sodium (0.9 ml/100g). For the surgical procedures, a 3 mm diameter and 5 mm deep hole was made by a hand driller at the lateral epicondyle by a minimally invasive approach. BSNs powders were mixed with 1.5 wt% soldium alginate aqueous (SA) at a ratio of 1g BSNs: 3.5 ml SA and implanted into the hole, then the incisions were closed carefully. After the surgery, the rats were intraperitoneally injected with fluorochromes under anaesthesia as follows: 30 mg/kg alizarin red (Sigma, USA) on week 6 and 20 mg/kg calcein (Sigma, USA) on week 9. All rats were sacrificed by intraperitoneal injection with an overdose of hydrate sodium on week 12. The bones were extracted for further characterization.

2.4.4. Micro-CT

The bone samples were scanned with micro-computerized tomography (micro-CT, Skyscan 1176, Belgium) at a 100 kV/100 μA X-ray source with an isotropic voxel size of 18 μm. The reconstruct tomograms were created with a 3D Creator software (Skyscan Software). The ratio of bone volume/tissue volume (BV/TV), trabecular number (Tb. N), and trabecular space (Tb. Sp) of new bone were calculated.

2.4.5. Histological analysis

For VG, H&E and Masson's trichrome staining, the specimens were fixed in 10% formalin for 2 days, dehydrated with a graded series of ethanol and embedded in paraffin. The samples were sliced into 5 μm thick sections, which were afterwards stained with Van Gieson Staining, Hematoxylin-Eosin and Masson's Trichrome Stain Kit (Solarbio, China), then examined with an optical microscope (Leica). For fluorescence labelling, the specimens were dehydrated in a graded alcohol series for 7 days and then embedded in methyl methacrylate without decalcification. The non-decalcified samples were cut with a diamond saw (SP1600, Leica) and ground to approximately 150 μm in thickness. To observe the fluorescence labelling, the specimens were observed with a confocal laser scanning microscope (Leica). For VG staining, the specimens stained with Van Gieson Staining were observed with an optic microscope (Leica).

2.4.6. Immunohistochemical staining

After samples were decalcified in 10% ethylenediaminetetraacetic acid (EDTA; Sinopharm Chemical Reagent Co., Ltd) for 14 days, they were embedded in paraffin and sectioned into 5 μm thick slices at the central area of the defect. For immunohistochemical staining, sections were first incubated with primary antibody OCN (GB11233, Servicebio, China) and CD31 (GB12063, Servicebio, China) at 4 °C overnight and then incubated with secondary antibody for 1 h. Afterwards, the diaminobenzidine (Dako, Danmark) were used to develop the color reaction. Finally, the sections were observed under a light microscope (Leica).

2.5. Anti-tumor evaluation

2.5.1. Hydroxyl radical (·OH) generation

The ability of BSNs to generate hydroxyl radicals in a simulated tumor microenvironment was characterized by the degradation and discoloration of methyl blue solution [24]. In brief, methyl blue was dissolved in PBS solution with different pH values (pH = 6.0 and pH = 8.0) at a concentration of 10 μg/ml, then glutathione and hydrogen peroxide were sequentially added to the methyl blue solution at a concentration of 10 mM and 20 mM respectively. Then BSNs were dispersed in the above solution at a concentration of 400 μg/ml. After a certain period of time, the absorption of the solution was tested using UV–Vis spectrophotometer (U3310, Hitachi), and the change of the absorption spectrum with time was used to assess the generation of hydroxyl radicals.

2.5.2. Tumor cells cytotoxicity in vitro

The cytotoxicity of BSNs to hBMSCs and mouse osteosarcoma cell line (143B) was studied by CCK-8 [23]. Briefly, the two kinds of cells were planted in 96-well plates (1×10^4 cells in 100 μl a-MEM per well) (n = 6), and the cells were cultured for 24 h and then 10 μl of suspension with different content of BSNs were added (the final concentration of BSNs was 500, 400, 300, 200, 100, 50, 25, 10, 5 μg/ml), 10 μl of ultrapure water was added as a blank control. After 24h of incubation, the medium was removed and each well was washed with PBS, then 100 μl of fresh FBS-free medium containing 10% CCK-8 (Cell Counting Pack, Beyotime, China) was added. After 2h of incubation, OD @450 nm was tested by a microplate reader (TECAN, Switzerland), and the relative cell viability was calculated based on the blank control.

2.5.3. Intracellular hydroxyl radical generation

In order to study the level of reactive oxygen species produced when BSNs interact with cells, the reactive oxygen species detection kit (S0033S, Beyotime Biotechnology, China) was used to test the production of intracellular hydroxyl radicals [33]. The specific method is as follows: 2×10^4 143B cells in 500 μl a-MEM were planted in a 48-well plate for 24h, then 50 μl of BSNs suspension were added with the final concentration of 100 μg/ml (n = 3). After 12h of incubation, the medium was removed, and each well was washed twice with PBS and then diluted DCFH-DA (1:1000) was added to each well to obtain a concentration of 10 μM according to the manufacturer's manual. After being incubated at 37 °C for 20 min, each well was wash three times with serum-free medium, and then observed with a fluorescence microscope (Olympus, Japan).

2.5.4. Anti-tumor in vivo

Twenty BALB/c female mice (7 weeks old) used in this experiment were purchased from Beijing Weitong Lihua Experimental Animal Co., Ltd. All the procedures were performed in Shenzhen Institutes of Advanced Technology (SIAT), Chinese Academy of Sciences, in accordance with the Animal Research Committee of SIAT (SIAT-IACUC-200211-YYS-PHB-A1022) [34]. After arrival, the animals were acclimated for 7 days prior to the study. The hair on the back of the mouse was shaved, and 100 μl of Matrigel PBS solution containing 143B cells (1×10^7 cells/ml) was subcutaneously injected into the back of the mouse. When the tumor grew to 100–120 mm^3 (The tumor volume was calculated by formula $V = L \times W^2/2$ (V, the tumor volume; L, the longest dimension; W, the shortest dimension)), the mice were equally divided into 5 groups, and these tumor bearing mice were treated with (1) saline, (2) 2 μg/g DOX, (3) 10 μg/g BSNs-Cu, (4) 10 μg/g BSNs-Mn and (5) 10 μg/g BSNs-Cu-Mn respectively via intratumoral administration (A dosage of 2 μg/g DOX was chosen as a positive control group because the concentration has become an accepted and established therapeutic procedure in the research of the osteosarcoma [35]; a dosage of 10 μg/g BSNs-Cu/BSNs-Mn/BSNs-Cu-Mn was used to treat tumor because 10 μg/g BSNs was the minimal dose for the depression of osteosarcoma in the pre-experiments). The injection was repeated every 2 days. Meanwhile the body weight and tumor volume were recorded. After 14 days, all of the mice were sacrificed, and the tumors and main organs were excised for further characterization. The tumors were photographed and then fixed for H&E staining. And terminal deoxynucleotidyl transferase-mediated dUTP nick-end labeling (TUNEL) staining analysis was performed for apoptosis analysis of the cancer cells. The results were observed by fluorescence microscopy. For biosafety assessment, the major organs, including heart, liver, spleen, lung and kidney, were sliced and analyzed using H&E staining.

2.6. Statistical analysis

Data were expressed as mean ± SD. Difference between groups was determined by one-way ANOVA and were deemed statistically significant when $p < 0.05$ (* means $p < 0.05$, **means $p < 0.01$).

3. Results

3.1. Characterization of BSNs

The preparing process of BSNs was illustrated in Fig. 1A. The characteristic properties of the prepared four type of particles were analyzed by XRD (Fig. 1B), and the results showed only broad peaks appeared in the XRD patterns, which indicated amorphous borosilicate bio-ceramics were successfully synthesized. FTIR was also applied to examine the structure of the prepared borosilicate particles (Fig. 1C), and the FTIR spectrum suggested several absorbance bands of borosilicate, in which the peaks at 1060 and 805 cm^{-1} were attributed to the vibration of [Si–*O*–Si] and the peaks at 1393 and 942 cm^{-1} were associated with the vibration of [B–*O*–B] [36].The morphology of these four types of borosilicate particles were observed by TEM (Fig. 1D), and TEM images indicated that the prepared materials were nanoparticles with an average particle size of about 50 nm, and due to the sintering process, BSNs show different degrees of agglomeration, but as a locally used material, this degree of agglomeration has no significant negative impact. Meanwhile ICP-OES was conducted to analyze the composition of the prepared nanoparticles, which was presented in Table 1. Furthermore, XPS was used to examine the valence of copper and manganese incorporated in the network of borosilicate (Fig. 1E–H). Through the analysis of XPS spectrums, it was confirmed that copper existed in the form of Cu(II) [34]; most manganese existed in the form of Mn(III), and a small amount existed in the form of Mn(Ⅳ) [33,37,38]. So far, we believed that borosilicate nanoparticles (BSNs) had been successfully synthesized in this work.

Mineralization activity, the ability of BSNs inducing the formation of apatite in simulated body fluids, was also characterized by XRD (Fig. 2A) and SEM (Fig. 2B). XRD patterns showed the characteristic peaks of apatite, and SEM images indicated the formation of apatite on the surface of BSNs, and apatite formed on BSNs-Cu and BSNs-Cu-Mn were the most obvious among groups. Both XRD and SEM demonstrated that BSNs could induce the formation of apatite, showing the potential as bone repairing materials. And to verify the activity of BSNs, ICP-OES was used to evaluate the ion releasing of BSNs in simulated body

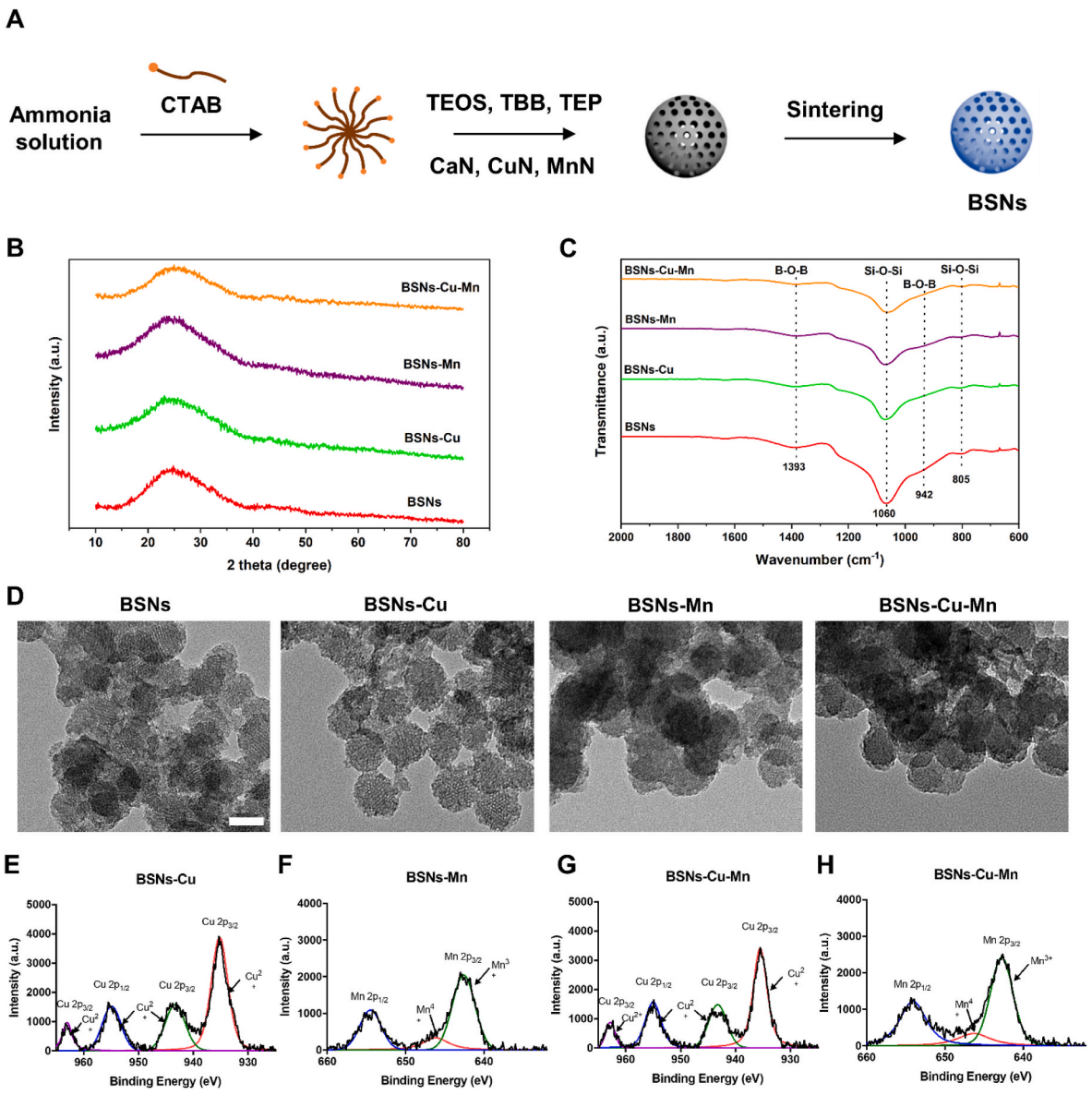

Fig. 1. Characterization of BSNs. (A) Diagram of the preparation of BSNs through sol-gel soft template method. **(B)** XRD patterns of the prepared four types of BSNs. The broad peaks indicated the amorphous structure of BSNs. **(C)** FTIR spectrum of BSNs. The peaks at 1060 and 805 cm^{-1} were attributed to the vibration of [Si–*O*–Si] and the peaks at 1393 and 942 cm^{-1} were associated with the vibration of [B–*O*–B]. **(D)** TEM images of the prepared BSNs. They showed BSNs were mesoporous dispersed nanoparticles which are distributed around 50 nm in particle size; scale bar: 50 nm. **(E)** Cu 2p XPS spectrum of BSNs-Cu. **(F)** Mn 2p XPS spectrum of BSNs-Mn. **(G)** Cu 2p XPS spectrum of BSNs-Cu-Mn. **(H)** Mn 2p XPS spectrum of BSNs-Cu-Mn. The XPS spectrums of BSNs confirmed that copper existed in the form of Cu(II); most manganese existed in the form of Mn(III), and a small amount existed in the form of Mn(IV).

Table 1
The composition of BSNs calculated from ICP-OES data.

Composition (wt %)	BSNs	BSNs-Cu	BSNs-Mn	BSNs-Cu-Mn
Si	91.0	77.8	76.1	60.2
B	1.9	1.3	1.5	1.5
Ca	6.6	6.3	7.0	9.6
P	0.5	0.4	0.8	0.6
Cu	–	14.2	–	16.0
Mn	–	–	14.6	12.1

fluids (Fig. 2C–F). The releasing profile of B, Si, Cu and Mn indicated that since these ions are in different positions in the glass structure (Si and B are network formers [13], Cu and Mn are network intermediates [39,40]), the release behavior of Si and B are similar to certain degree, and both are relatively slow; and due to the different effects of Cu and Mn on the glass structure (Cu are found to strengthen the glass network [41]), the release behavior of these two ions present different trends, and the release of Cu^{2+} becomes slower than Mn^{3+} in the later stage. But overall BSNs can gradually release various therapeutic ions, thereby ensuring their bioactivity when interacting with cells or tissues.

3.2. Bone repairing evaluation

3.2.1. Osteogenesis of rBMSCs and angiogenesis of EaHy926 in vitro

The effects of BSNs on the proliferation of rBMSCs *in vitro* were assessed by CCK-8 (Fig. 3A). The results showed that the four types of BSNs were not toxic to rBMSCs and promoted cell proliferation to varying degrees. Among them, the promotive effect of BSNs doped with Cu and Mn was particularly significant, which resulted from the dual effects of Cu^{2+} and Mn^{3+} ions. And the osteogenic differentiation of rBMSCs was also characterized by detecting ALP activity (Fig. 3B). It's

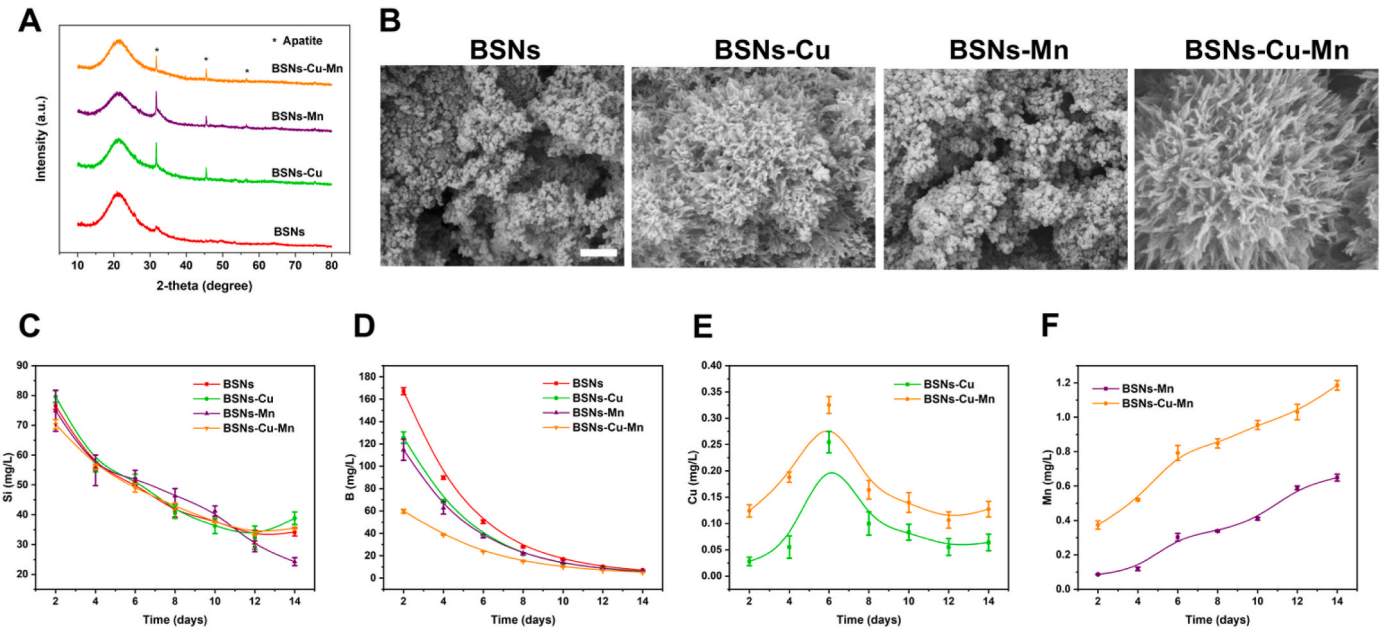

Fig. 2. Bioactivity of BSNs. (A) XRD patterns of BSNs soaked in SBF for 7 days. It indicated the presence of apatite. **(B)** SEM images of the surface of BSNs soaked in SBF for 7 days; scale bar: 500 nm. It showed the presence of apatite, and apatite formed on BSNs-Cu and BSNs-Cu-Mn were the most obvious among groups. **(C)** Si, **(D)** B, **(E)** Cu and **(F)** Mn ions releasing profile of BSNs determined by ICP-OES. It indicated that BSNs can gradually dissolve and release therapeutic ions.

shown that all of the four types of BSNs improved the ALP activity, and BSNs-Cu-Mn took the lead, indicating the ability of Cu^{2+} and Mn^{3+} to promote osteogenic differentiation. The expression of osteogenesis-related genes was determined by RT-PCR (Fig. 3C–E), which showed the BSNs incorporated with Cu and Mn upregulated the expression of osteogenesis-related genes including BMP2, COL1A1 and RUNX2, indicating the ability of Cu/Mn doped BSNs to promote osteogenesis. Furthermore, ALP and Alizarin red stainings on day 21 were also conducted to evaluate the osteogenic differentiation of rBMSCs (Fig. 3F and G), which showed a similar trend to ALP activity and BSNs doped with Cu and Mn promoted the osteogenesis of rBMSCs significantly, which further demonstrated the promotive effects of Cu^{2+} and Mn^{3+} on the osteogenesis of BMSCs. All these results confirmed that Cu and Mn can further improve the osteogenic capacity of borosilicate nanoparticles.

To study the angiogenesis of EaHy926, firstly, the effects of four types of BSNs on the proliferation of EaHy926 were determined by CCK-8 (Fig. 4A), and the results showed all BSNs were compatible with cells and promoted cell proliferation. Meanwhile the expression of VEGF was quantified by an Elisa kit (Fig. 4B). And the result showed that BSNs-Cu and BSNs-Cu-Mn obviously improved the VEGF activity. Furthermore, transwell and tube formation assays were used to study the migration and tube formation of EaHy926 (Fig. 4C), it's shown that BSNs incorporated with Cu and Mn can significantly promote the migration and tube formation of EaHy926 *in vitro* except for BSNs-Mn, which had no significant promoting effect on tube formation. All these results are in line with the conclusions of previous studies [42,43].

3.2.2. Bone formation capacity of BSNs

The bone formation capacity of BSNs was estimated by the repairing of lateral epicondyle defects of rats. The bone formation was evaluated by Micro-CT (Fig. 5A, 5C-E). The 2D and 3D reconstruction photos and the calculated BV/TV, Tb. N and Tb.Sp showed that BSNs-Cu and BSNs-Cu-Mn promoted more bone formation among the groups after 12 weeks. The number of trabecular in the BSNs-Cu and BSNs-Cu-Mn group were also higher, and the trabecular spacing were smaller. These results indicated that the incorporation of Cu and Mn could further promote bone regeneration, and the effect of BSNs containing copper were particularly significant.

The newly formed bone tissue after BSNs were implanted was also marked by fluorescence labeling (Fig. 5B and F), specifically calcein (green) and alizarin red (red). The results showed that in BSNs-Cu and BSNs-Cu-Mn group, the fluorescence intensity and the fluorescence distribution area were higher than those of the other groups, indicating that BSNs-Cu and BSNs-Cu-Mn have the higher osteogenic ability, which was consistent with the results of Micro-CT.

VG, H&E and Masson staining were used to analyze the structure of newly formed bone tissue (Fig. 6A–C). As the results showed, more bone and collagens were regenerated in BSNs-Cu and BSNs-Cu-Mn group particularly in the defect area. At the same time, immunohistochemical staining of the osteogenic related proteins OCN and CD31 were conducted to reveal the osteogenesis and angiogenesis in the bone repairing process (Fig. 6D and E), and the results showed that positive brown staining for OCN were more apparent in BSNs-Cu and BSNs-Cu-Mn group, indicating the higher bone formation ability of BSNs-Cu and BSNs-Cu-Mn. And the positive staining for CD31 showed that more blood vessels were formed in BSNs-Cu and BSNs-Cu-Mn group. Both OCN and CD31 staining demonstrated that BSNs-Cu and BSNs-Cu-Mn promoted bone repairing with improved bone regeneration and blood vessel formation, which might be due to the dual effects of Cu and Mn ions on osteogenesis and angiogenesis.

3.3. Anti-tumor evaluation

3.3.1. Production of hydroxyl radicals in a simulated tumor microenvironment

The ability of BSNs to generate hydroxyl radicals in a simulated tumor microenvironment was characterized by the degradation and discoloration of methyl blue solution (MB) (Fig. 7A). For the four kinds of BSNs, the changing trend of the absorbance of MB were not consistent. BSNs would not cause discoloration of MB under acidic or alkaline conditions. BSNs-Cu caused the color fading of MB under acidic condition but didn't cause discoloration of MB under alkaline condition. BSNs-Mn caused the color fading of MB under both acidic and alkaline conditions. And BSNs-Cu-Mn showed a similar impact on MB as BSNs-Cu, which caused the color fading of MB under acidic condition but didn't cause the discoloration of MB under alkaline condition. These

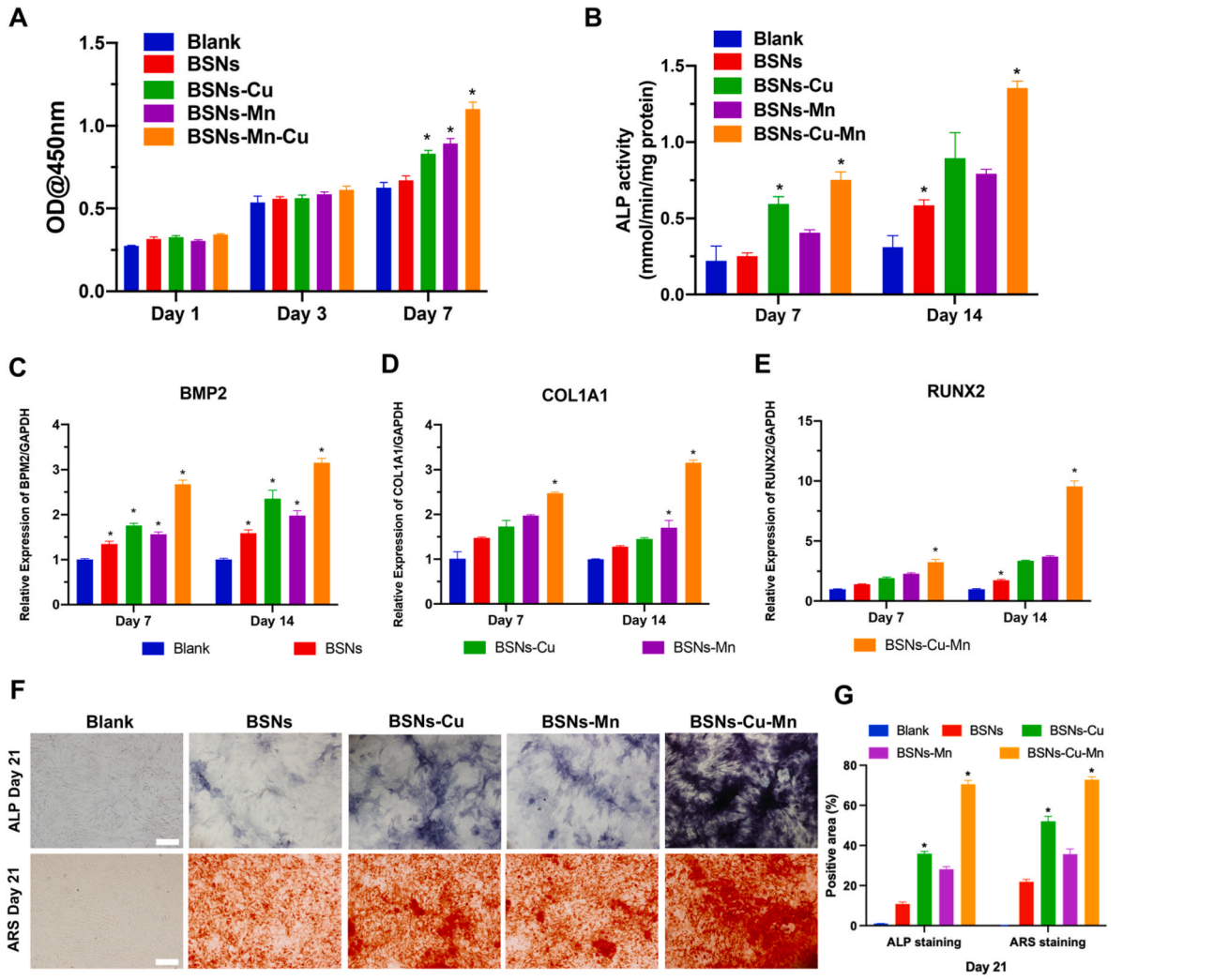

Fig. 3. Osteogenesis in *vitro*. (A) The proliferation of rBMSCs tested by CCK8. rBMSCs showed good viability and maintained the potential to continue to proliferate. **(B)** ALP activity determined by ALP kit. It indicated that doped BSNs promoted the expression of ALP, especially for BSNs doped with copper. **(C–E)** The expression of osteogenesis-related genes including BMP2 **(C)**, COL1A1 **(D)** and RUNX2 **(E)** assessed by RT-PCR. All the osteogenesis-related genes were upregulated under the effects of BSNs, and the effect of BSNs-Cu-Mn was particularly significant. **(F)** ALP staining and ARS staining on day 21; scale bars: 100 μm. It showed BSNs doped with copper significantly promoted the osteogenesis of rBMSCs *in vitro*. (G) Quantified positive area of ALP and ARS staining. (n = 3, $P < 0.05$, one-way ANOVA was used for statistical analysis.)

results indicated that the Fenton-like reactions of BSNs-Cu and BSNs-Cu-Mn were acid-dependent and tumor microenvironment-sensitive, which endowed BSNs-Cu and BSNs-Cu-Mn the potential for anti-tumor specifically.

The reactions involved in the generation of hydroxyl radicals were illustrated by Eq. (1)–(4). Cu (II) was firstly reduced by GSH to Cu (I) (Eq. (1)), Cu(I) then reacted with H_2O_2 to generate hydroxyl radicals (Eq. (2)). Similarly, Mn (IV) was reduced by GSH to Mn (II) (Eq. (3)), and Mn (II) continued to react with H_2O_2 to generate hydroxyl radicals (Eq. (4)). The discoloration of MB at different pH values above illustrated the effects of pH on Fenton-like reactions of Cu^{2+} and Mn^{3+}. Cu^{2+} ions require certain acidic conditions, while Mn^{3+} did not, which was consistent with the conclusions in the literature [24,44]. The tumor microenvironment can just meet the requirements and promote the generation of hydroxyl radicals through Fenton-like reaction of BSNs-Cu and BSNs-Cu-Mn, which would in turn promote tumor cell apoptosis.

$$Cu^{2+} + GSH \rightarrow Cu^{+} + GSSG \quad (1)$$

$$Cu^{+} + H_2O_2 \rightarrow Cu^{2+} + \cdot OH + OH^{-} \quad (2)$$

$$Mn^{3+} + GSH \rightarrow Mn^{2+} + GSSG \quad (3)$$

$$Mn^{2+} + H_2O_2 \rightarrow Mn^{3+} + \cdot OH + OH^{-} \quad (4)$$

3.3.2. *Cytotoxicity of BSNs to tumor cells*

The cytotoxicity of BSNs to hBMSCs and 143B were determined by CCK-8 (Fig. 7B). The results showed that the four kinds of BSNs had different effects on hBMSCs and 143B: Undoped BSNs (BSNs) showed no cytotoxicity to both hBMSCs and 143B within the concentration range of 0-500ug/ml, and even promoted cells proliferation; BSNs-Cu was completely not toxic to hBMSCs below 400ug/ml, and even promoted cell proliferation. Only at high concentrations BSNs-Cu showed certain toxicity. However, BSNs-Cu had a significant inhibitory effect on 143B. As the concentration of BSNs-Cu increased, the cell viability of 143B gradually decreased; BSNs-Mn had the same inhibitory effect on hBMSCs and 143B cells; BSNs-Cu-Mn exhibited the same trend as BSNs-Cu. These findings indicated that Cu^{2+} can significantly inhibit tumor cells and is friendly to hBMSCs, while Mn^{3+} has a consistent effect on tumor cells and normal cells. The specific effect of Cu^{2+} on tumor cells endows Cu-doped borosilicate nanoparticles the great potential for osteogenic and

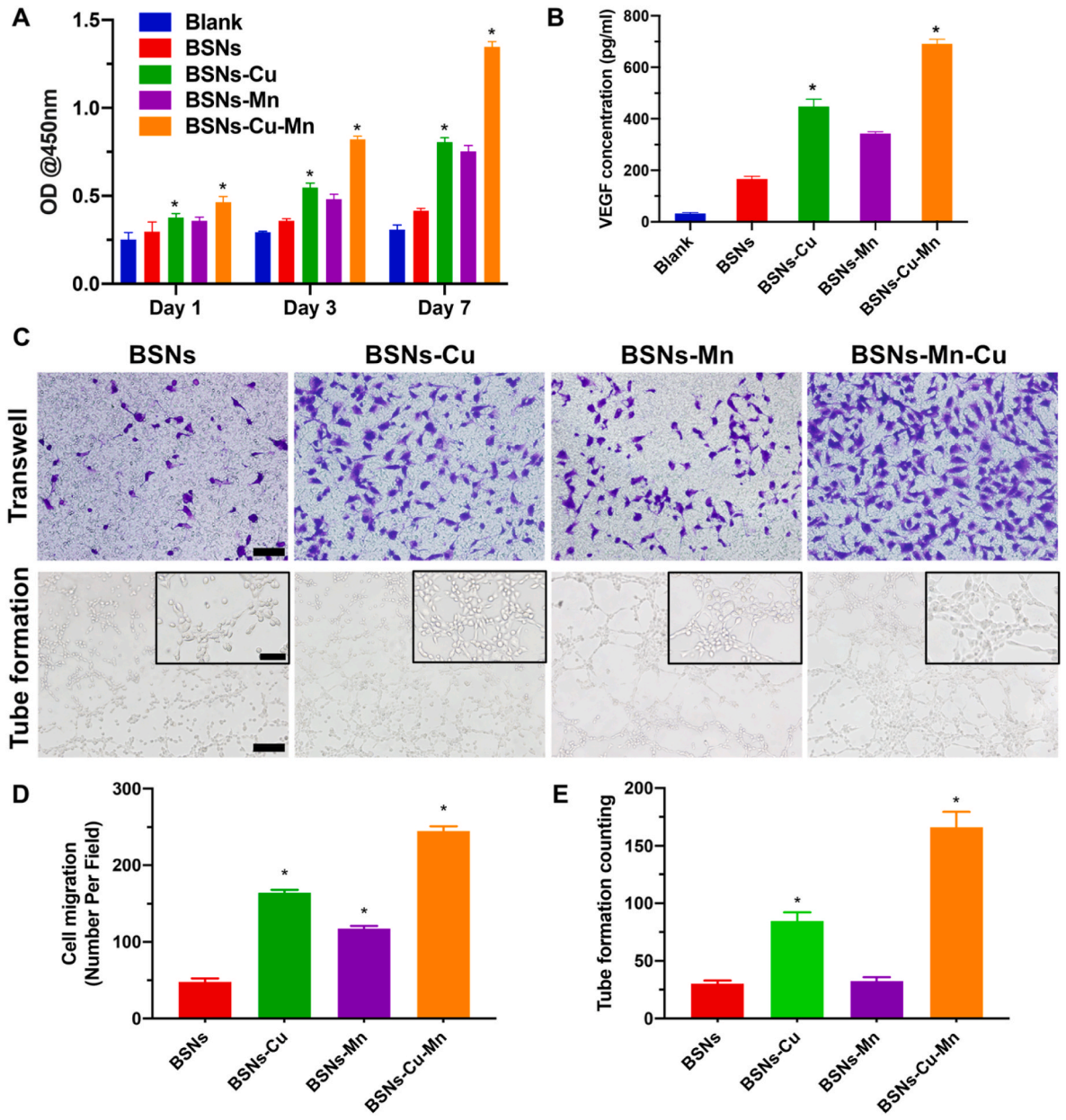

Fig. 4. Angiogenesis *in vitro*. (A) The proliferation of EaHy926 tested by CCK-8 (n = 6). It showed that BSNs promoted the proliferation of EaHy926, especially for BSNs doped with copper and manganese. **(B)** VEGF secrete assessed by Elisa kit (n = 3). It indicated that BSNs upregulated the expression of angiogenesis-related factor such as VEGF. **(C)** Transwell and tube formation assay of EaHy926; scale bars: 100 μm (scale bars in insets: 40 μm). **(D)** Quantified results of transwell assay. **(E)** Quantified results of tube formation assay. The results of transwell and tube formation assays showed that BSNs containing copper promoted the migration and tube formation of EaHy926, indicating their high potential for angiogenesis enhancement. (*P < 0.05, one-way ANOVA was used for statistical analysis.)

anti-tumor applications.

Furthermore, the generation of intracellular hydroxyl radicals were detected by a ROS detection kit (Fig. 7C). The results showed the green fluorescence intensity of the cells treated with BSNs-Cu, BSNs-Mn and BSNs-Cu-Mn were much higher, indicating that BSNs-Cu, BSNs-Mn and BSNs-Cu-Mn can significantly increase the level of intracellular ROS, thereby having a stronger tumor cell killing effect.

3.3.3. *Anti-tumor efficiency*

The anti-tumor effects of BSNs-Cu, BSNs-Mn and BSNs-Cu-Mn were evaluated by examining the size of subcutaneous tumors on mice. The body weight of tumor-bearing mice and tumor volume were recorded in the whole process of anti-tumor treatment (Fig. 8A and B). The weight of mice injected with saline increased slightly, and the weight of mice injected with DOX decreased slightly, while the weight of mice injected with BSNs did not change significantly, indicating the good growing status of mice. The tumors of mice injected with saline increased significantly, and the tumors of mice injected with DOX decreased significantly, while the tumors of mice injected with BSNs increased slightly, and there was no statistical difference among BSNs-Cu, BSNs-Mn and BSNs-Cu-Mn group, indicating that BSNs incorporated with Cu and Mn can inhibit tumor growth.

After the mice were sacrificed, the tumors were extracted and photographed (Fig. 8D), then fixed for H&E staining and terminal deoxynucleotidyl transferase-mediated dUTP nick-end labeling (TUNEL) staining to analyze apoptosis of the tumor cells (Fig. 8C). As the results showed, tumors treated with saline had no obvious apoptosis in both H&E and TUNEL staining; tumors treated with DOX had a wide range of cell apoptosis; tumors treated with BSNs also had obvious tumor cell apoptosis, which indicated that BSNs including BSNs-Cu, BSNs-Mn and

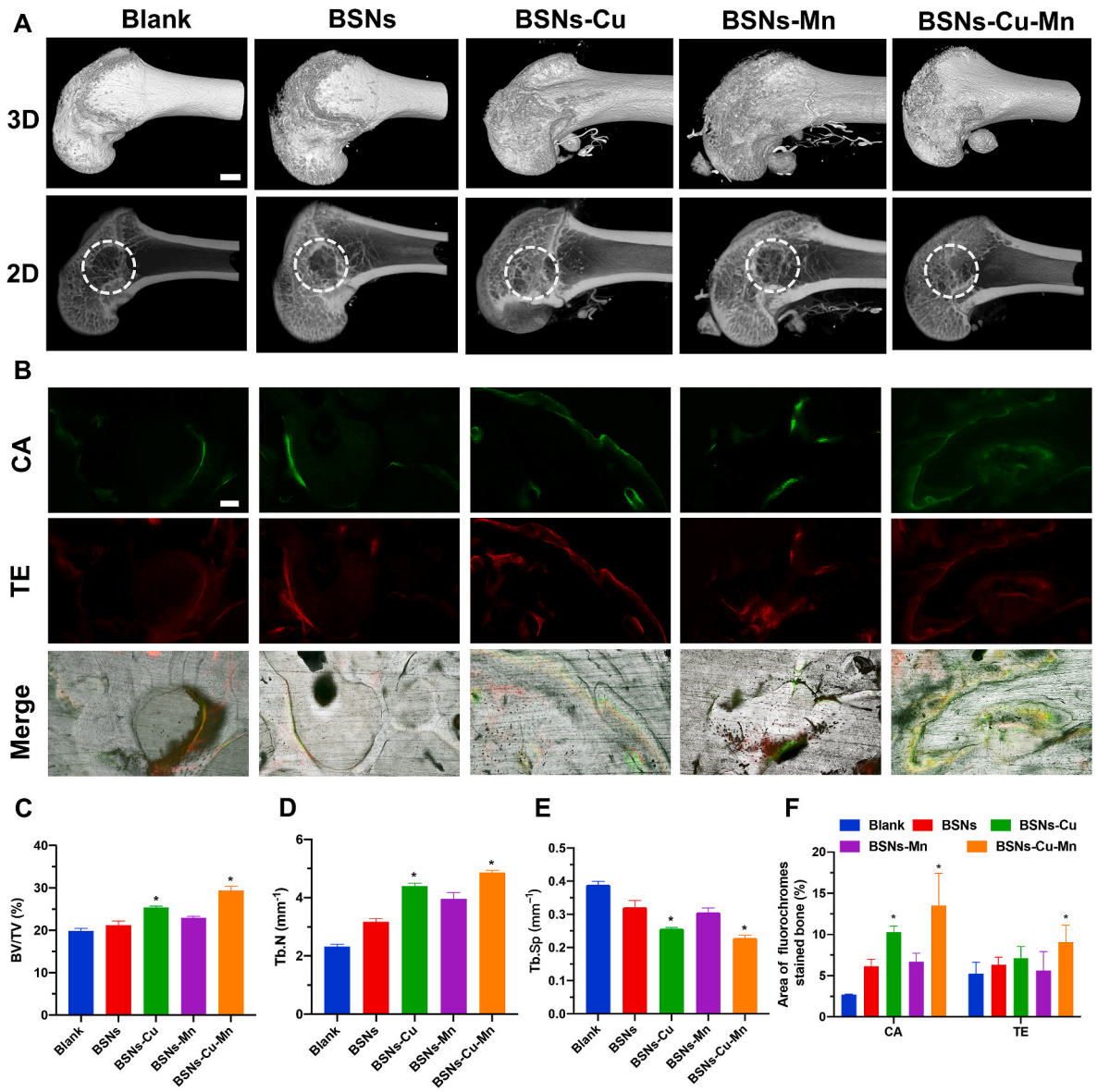

Fig. 5. Bone formation assay. (A) Micro-CT analysis; scale bar: 1 mm. **(B)** New bone formation marked by fluorochromes, scale bar: 100 μm. **(C)** Bone volume/tissue volume (BV/TV), **(D)** trabecular number (Tb. N) and **(E)** trabecular space (Tb. Sp) calculated from Micro-CT. **(F)** Quantified area of fluorochromes stained bone. All these findings showed BSNs containing copper significantly promoted the new bone formation, indicating their capacity for bone repairing. (n = 3, *P < 0.05, one-way ANOVA was used for statistical analysis.)

BSNs-Cu-Mn can effectively cause tumor cell apoptosis, thereby inhibiting tumor growth.

Furthermore, for biosafety assessment of BSNs injected into the body, the major organs of mice, including heart, liver, spleen, lung and kidney, were sliced and analyzed using H&E staining (Fig. 8E). The results showed that BSNs did not cause damage to the main organs of mice, indicating the biological safety of BSNs for anti-tumor therapy.

4. Discussion

As mentioned earlier, the repairing of bone defects and the removal of residual tumor cells after bone tumor surgery are challenges in the treatment of bone tumors. Herein we innovatively propose to develop copper (Cu) and manganese (Mn) doped borosilicate nanoparticles (BSNs) to address the issue, and the resulting Cu/Mn-doped BSNs can achieve not only enhanced osteogenesis and angiogenesis for bone regeneration, but also the ability of killing tumor cells due to hydroxyl radicals produced by Fenton-like reactions of Cu^{2+} and Mn^{3+}. In this study, we tried to build up two types of animal model to respectively evaluate the effects, since an actual bone osteosarcoma implantation model is technically challenging [45], for example, the number of residual tumor cells after osteosarcoma resection cannot be kept consistent between animals, which will have a huge impact on the experimental results. Moreover, due to the uncontrollable number of residual tumor cells, it is difficult to evaluate the anti-tumor performance of BSNs through observation of a few animals. Only through large-sample statistics can reliable results be obtained, which is not realistic at the laboratory stage. Through two separate animal models, we can at least relatively accurately evaluate the osteogenic properties and anti-tumor performance of BSNs, though it isn't perfect. According to the results we have achieved, it's believed that Cu/Mn doped BSNs holds potential for synergistic bone repairing and tumor therapy in bone tumor treatment (Fig. 9):

Firstly, for bone repairing, borosilicate nanoparticles (BSNs)

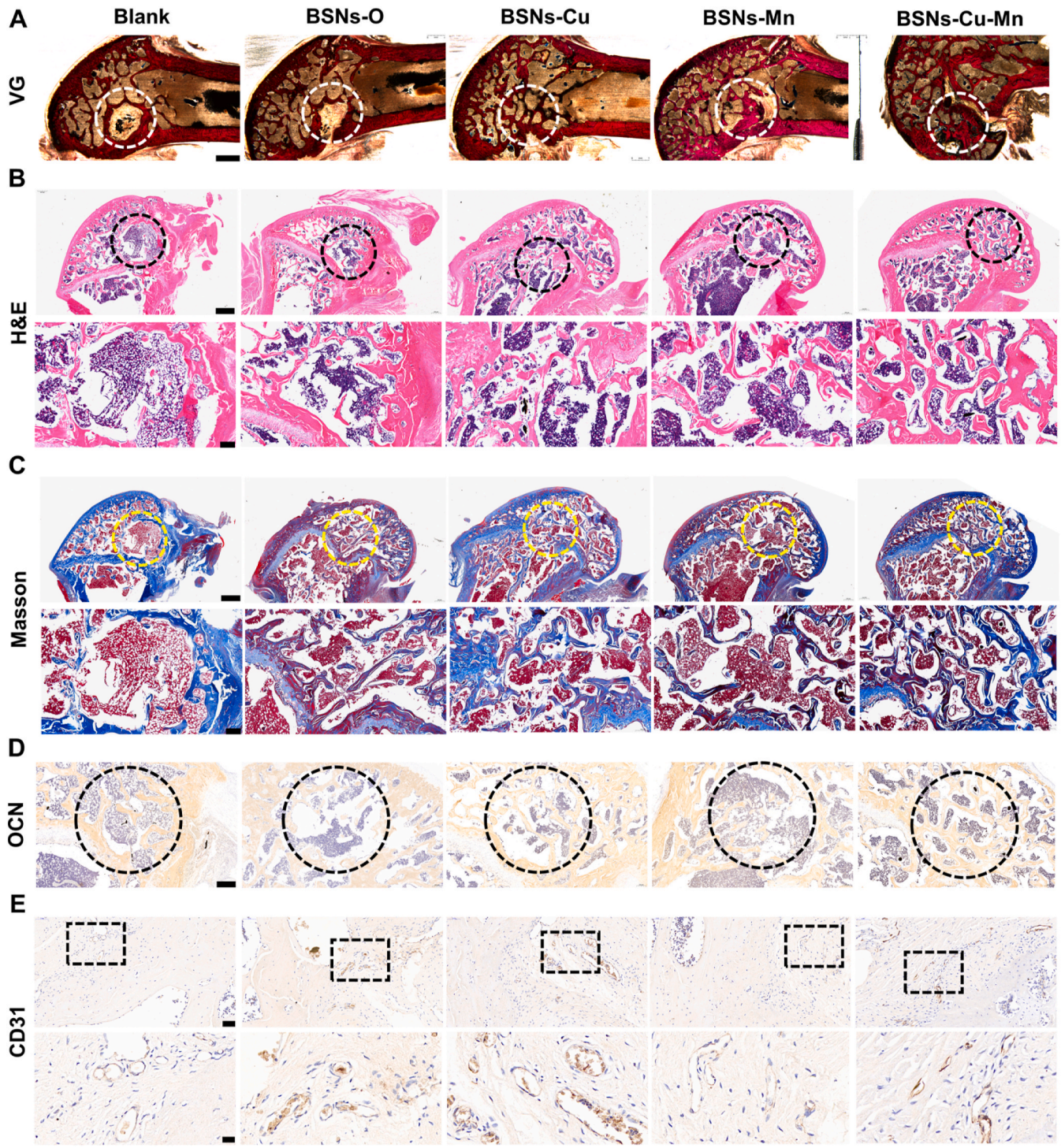

Fig. 6. Histological analysis for bone formation. (A) VG staining; scale bar:1 mm. **(B)** H&E staining; scale bar in upper row: 400 μm, scale bar in lower row: 100 μm. Both the results showed BSNs containing copper (BSNs-Cu and BSNs-Cu-Mn) promoted bone formation. **(C)** Masson staining; scale bar in upper row: 400 μm, scale bar in lower row: 100 μm. The results showed that in BSNs-Cu and BSNs-Cu-Mn group, more collagen fibers were formed, indicating better bone formation. **(D)** Immunohistochemical staining for OCN; scale bar: 400 μm. It showed that positive brown staining for OCN were more apparent in BSNs-Cu and BSNs-Cu-Mn group. **(E)** Immunohistochemical staining for CD31; scale bar in upper row: 50 μm, scale bar in lower row: 15 μm. The positive staining for CD31 showed that more blood vessels were formed in BSNs-Cu and BSNs-Cu-Mn group. Both OCN and CD31 staining demonstrated that BSNs-Cu and BSNs-Cu-Mn promoted bone repairing through enhanced osteogenesis and angiogenesis.

developed in this work is a dual network of interconnected [SiO_4] and [BO_3] groups, whose degradation behavior and functionality could be regulated by the adjustment of [SiO_4]/[BO_3] ratio and the incorporation of desirable therapeutical ions to promote bone formation [13]. Furthermore, borosilicate can also provide an alkaline local condition to stimulate the differentiation of bone marrow stem cells (BMSCs) into osteoblasts, as we published substantially in the past few years [16,19,46,47]. If the postulation is positive, borosilicate provides the basic environment for bone formation. The results in our study confirmed that BSNs can promote the proliferation and osteogenic differentiation of

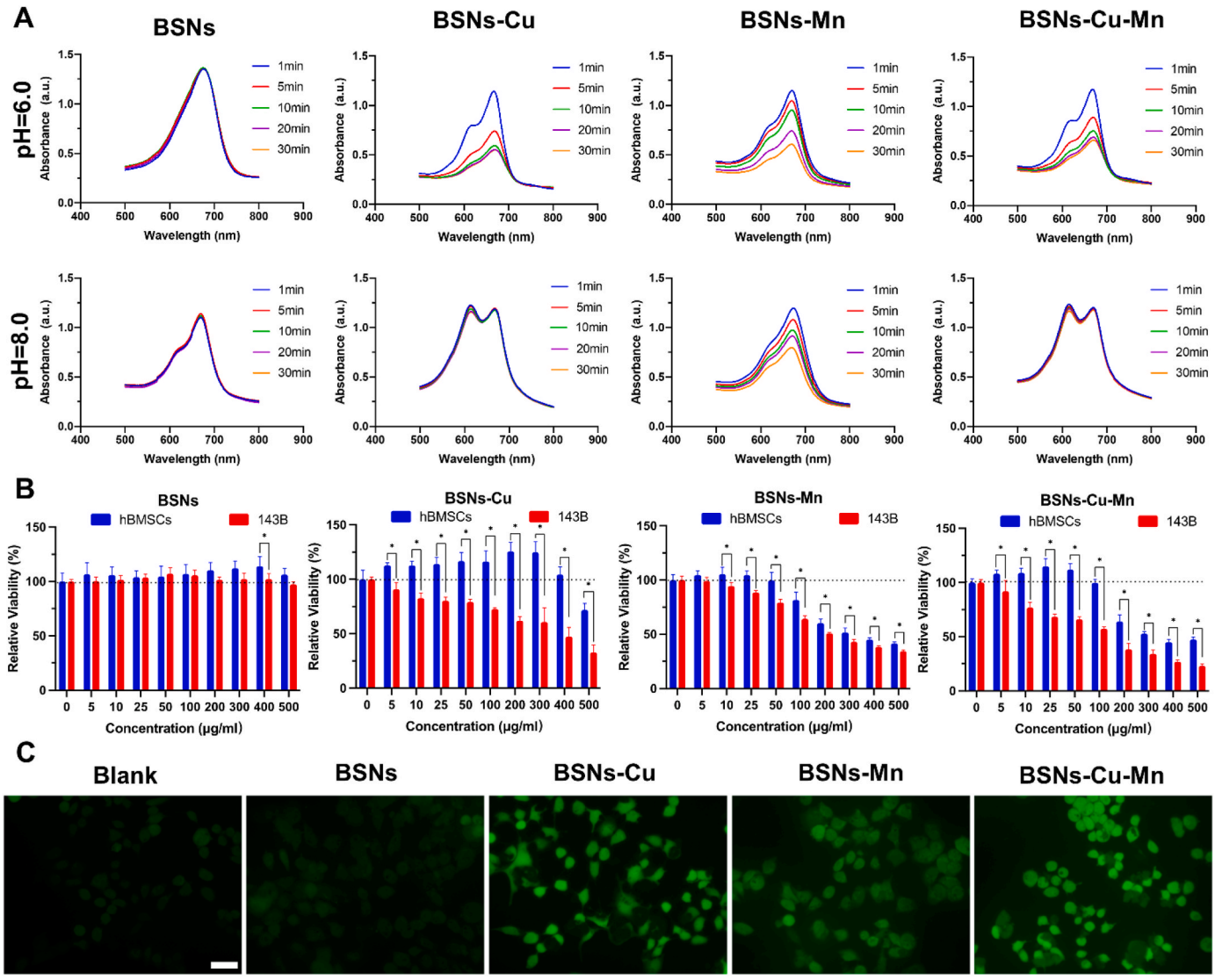

Fig. 7. Anti-tumor evaluation *in vitro*. (A) Production of hydroxyl radicals in a simulated tumor microenvironment characterized by the degradation and discoloration of methyl blue solution (MB). BSNs-Cu caused the color fading of MB under acidic condition but didn't cause discoloration of MB under alkaline condition; BSNs-Mn caused the color fading of MB under both acidic and alkaline conditions; BSNs-Cu-Mn caused the color fading of MB under acidic condition and didn't cause the discoloration of MB under alkaline condition. **(B)** Cytotoxicity of BSNs ($n = 6$, $^*P < 0.05$). BSNs showed no cytotoxicity to both hBMSCs and 143B within the concentration range of 0-500ug/ml, and even promoted cells proliferation; BSNs-Cu was completely not toxic to hBMSCs below 400ug/ml, and even promoted cell proliferation, and BSNs-Cu had a significant inhibitory effect on 143B. BSNs-Mn had the same inhibitory effect on hBMSCs and 143B cells; BSNs-Cu-Mn exhibited the same trend as BSNs-Cu. **(C)** Intracellular hydroxyl radicals detected by ROS kit ($n = 3$); scale bar: 50um. The green fluorescence intensity in the BSNs-Cu, BSNs-Mn and BSNs-Cu-Mn groups were much higher, indicating that BSNs-Cu, BSNs-Mn and BSNs-Cu-Mn can significantly increase the level of intracellular ROS, thereby having a stronger tumor cells inhibitory effect.

BMSCs, as well as the angiogenesis of endothelial cells, and showed an efficient repairing of rat bone defect models through improved osteogenesis and angiogenesis. Therefore, BSNs is capable of repairing bone defects caused by surgery.

Then for anti-tumor therapy, effective removal of tumor cells and inhibition of tumor growth are its criteria. Although chemotherapy and radiotherapy meet this criterion, they will cause relatively large side effects to the body. The anticipated approach is to develop new tumor therapies with less side effects to normal tissues, such as photothermal therapy and photodynamic therapy [48]. Among them, chemodynamic therapy (CDT) is a new concept that utilizes the Fenton-like reactions of Fe^{2+}, Cu^{2+}, Mn^{3+} ions etc. in the tumor microenvironment to generate hydroxyl radicals to trigger tumor cell apoptosis [22]. CDT does not require external intervention except for slight acidity and excessive hydrogen peroxide, and thereby can *in situ* inhibit tumor growth [49]. BSNs developed in this study have the unique tissue penetrability of nanoparticles, which can penetrate the surrounding tumor tissues, release Cu^{2+} and Mn^{3+} ions into the microenvironment of tumor tissue, then produce hydroxyl radicals through Fenton-like reactions, and finally induce tumor cell apoptosis. *In vitro* studies confirmed that Cu and Mn-doped BSNs can generate hydroxyl radicals in the simulated tumor microenvironment and promote the production of intracellular reactive oxygen species and cause tumor cell apoptosis. Furthermore Cu-incorporated BSNs were found to have a specific killing effect on tumor cells. The *in vivo* anti-tumor experiments also further demonstrated that Cu/Mn doped BSNs can effectively induce tumor cell apoptosis and inhibit tumor growth, while showing no toxic side effects to normal tissues and organs.

In summary, BSNs showed the dual effects both in bone formation and tumor inhibition. The therapeutic Si, B, Ca, P, Cu and Mn ions

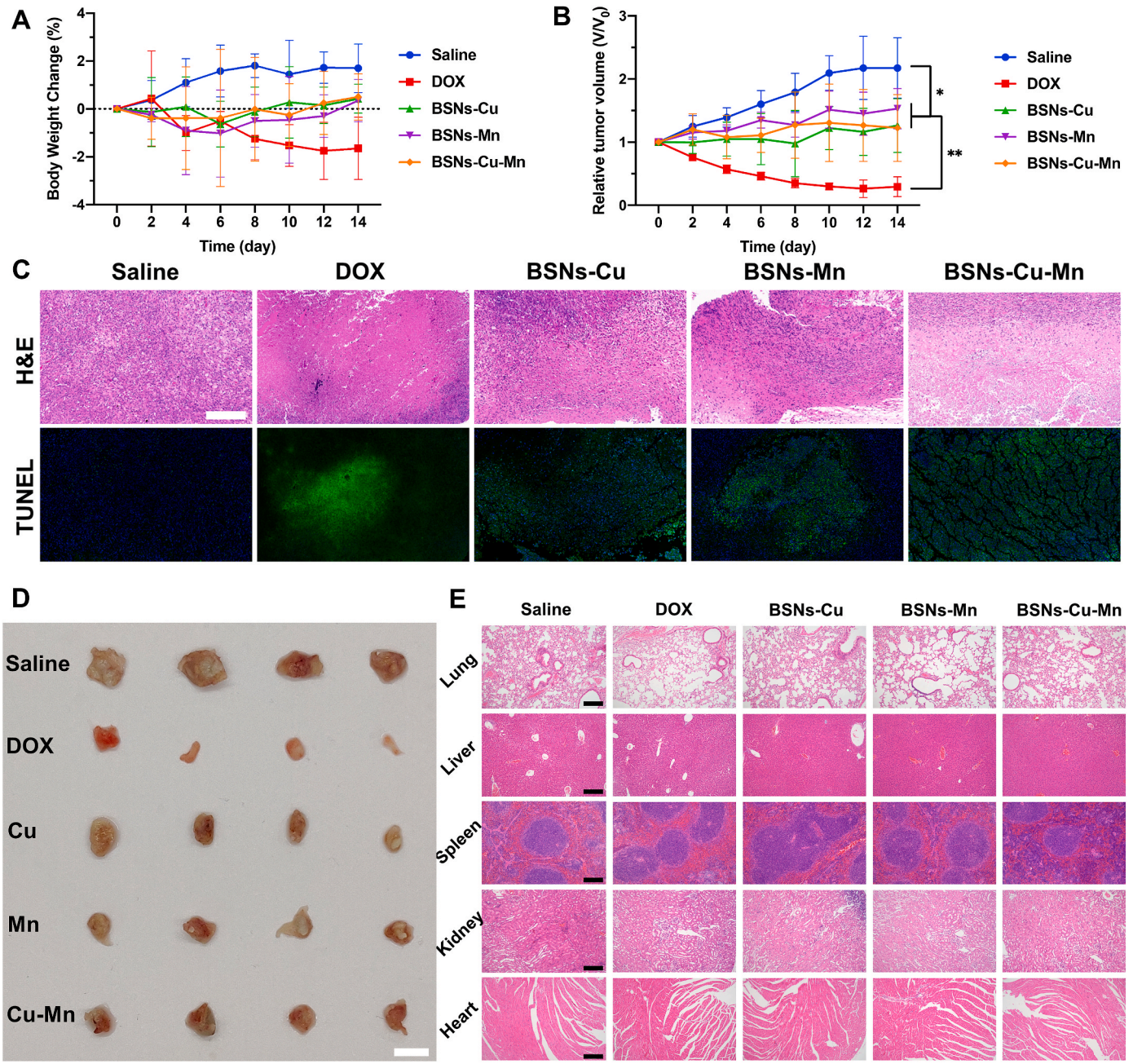

Fig. 8. Anti-tumor *in vivo*. (A) Weight change of mice with time. The weight of mice injected with Saline increased slightly, and the weight of mice injected with DOX decreased slightly, while the weight of mice injected with BSNs did not change significantly. **(B)** Relative tumor volume change with time. Tumors injected with injected with BSNs showed no significant growth, indicating that BSNs incorporated with Cu and Mn can inhibit tumor growth. **(C)** H&E and TUNEL staining for tumor tissue; scale bar: 100um. Both H&E and TUNEL staining showed tumors treated with Saline had no obvious apoptosis; tumors treated with DOX had a wide range of cell apoptosis; tumors treated with BSNs also had obvious tumor cell apoptosis. **(D)** Tumors extracted after the mice were sacrificed; scale bar: 1 cm. It also showed BSNs inhibited the tumor growth. **(E)** H&E staining for major organs; scale bars: 100um. The results showed that BSNs did not cause damage to the main organs of mice, indicating the biological safety of BSNs for anti-tumor therapy. (*P < 0.05, **P < 0.001, one-way ANOVA was used for statistical analysis.)

released from borosilicate network can promote osteogenesis and angiogenesis, thereby promoting bone repairing. Meanwhile, BSNs can penetrate tumor tissues to trigger Fenton-like reactions to produce hydroxyl radicals, causing tumor cell apoptosis and inhibiting tumor growth, and especially Cu-incorporated BSNs showed the specific killing effect on tumor cells. Such dual effects of Cu/Mn doped BSNs can not only induce bone regeneration but also induce tumor cells apoptosis, thus significantly improving the efficiency of bone repairing and reducing the risk of *in situ* tumor recurrence.

5. Conclusions

Copper and manganese doped borosilicate nanoparticles were successfully synthesized in this work, which can gradually release therapeutic ions including Si, B, Ca, Cu and Mn, and induce the formation of apatite in simulated body fluids, indicating high bioactivity for bone repairing. And *in vitro* and *in vivo* study confirmed the prepared Cu and Mn-doped BSNs can promote the proliferation and osteogenic differentiation of BMSCs, as well as the angiogenesis of endothelial cells, and showed an efficient *in vivo* bone defects repairing through improved osteogenesis and angiogenesis. Meanwhile, Cu and Mn-doped BSNs can

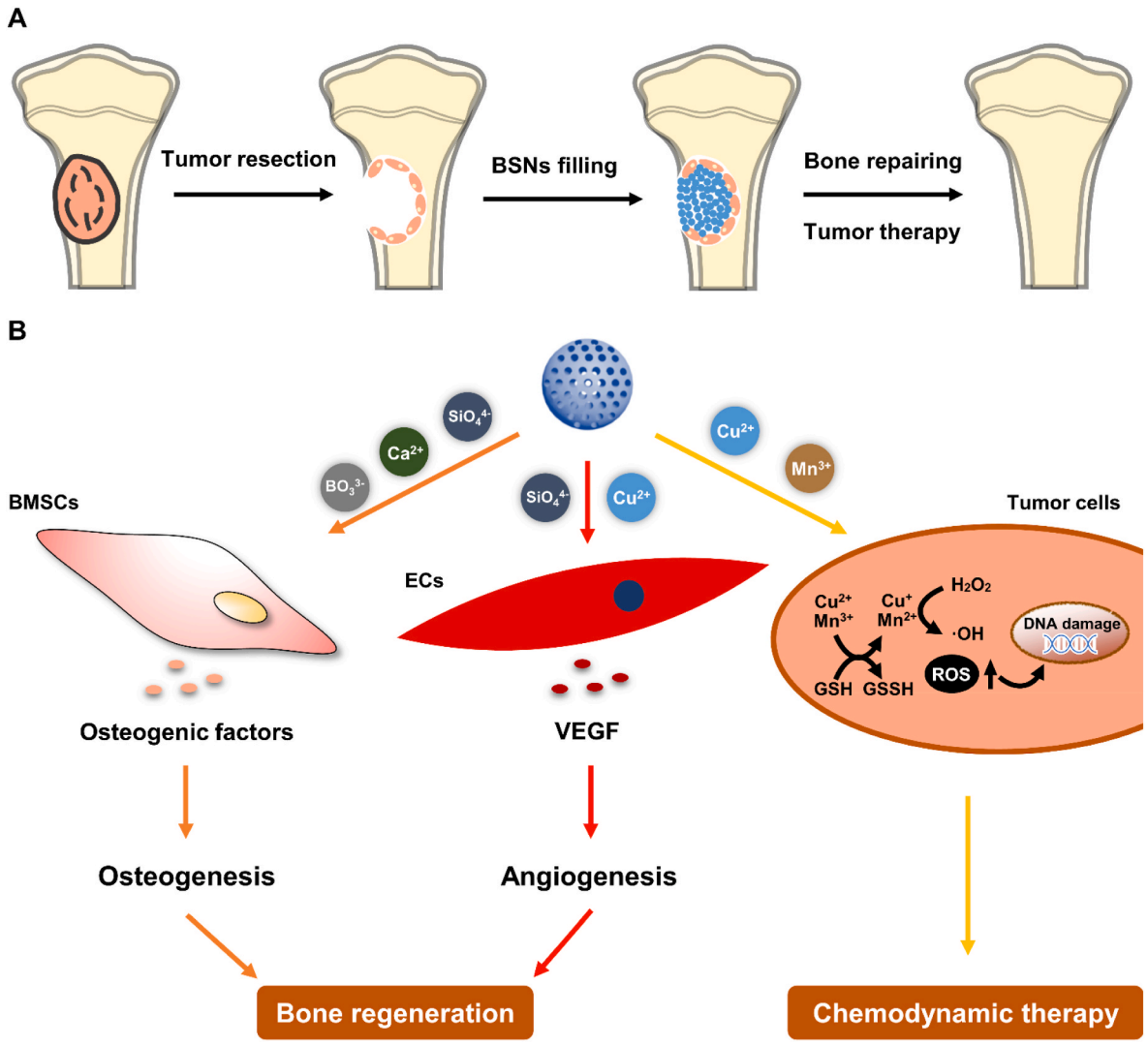

Fig. 9. Schematic illustration of BSNs for syncretic bone repairing and anti-tumor therapy. (A) Injectable BSNs filling bone defects after bone tumor resection. (B) BSNs for bone regeneration and anti-tumor therapy. BSNs can release various therapeutic ions including Si, B, Ca, P, Cu and Mn ions to promote the osteogenic differentiation of BMSCs and angiogenesis of endotheliocytes to enhance bone regeneration. Meanwhile, the released Cu and Mn ions will undergo Fenton-like reactions in tumor environment to produce hydroxyl radicals to induce tumor cell apoptosis (chemodynamic therapy), and thus remove residual tumor cells and avoid *in situ* tumor recurrence.

undergo Fenton-like reactions and generate hydroxyl radicals in the simulated tumor microenvironment, promote the generation of intracellular reactive oxygen species, and effectively induce tumor cell apoptosis and inhibit subcutaneous tumors of mice without causing toxic side effects to normal tissues and organs in the anti-tumor evaluation. Based on the bone repairing and anti-tumor evaluation in this work, Cu and Mn-doped BSNs are capable of repairing bone defects caused by bone tumor surgery through enhanced osteogenesis and angiogenesis and take advantages of the nanoparticles to penetrate the surrounding tumor tissues that remain after surgery to generate hydroxyl radicals through Fenton-like reactions of Cu^{2+} and Mn^{3+}, causing tumor cell apoptosis and inhibiting tumor tissue growth. Altogether, Cu and Mn-doped BSNs developed in this work hold the potential for syncretic bone repairing and chemodynamic therapy in the bone tumor treatment.

Declaration of interests

The authors declare that they have no known competing financial interests or personal relationships that could have appeared to influence the work reported in this paper.

The authors declare the following financial interests/personal relationships which may be considered as potential competing interests:

CRediT authorship contribution statement

Libin Pang: Conceptualization, Methodology, Writing – original draft. **Renliang Zhao:** Methodology, Formal analysis, Writing – review & editing. **Jing Chen:** Validation, Writing – review & editing. **Jingxin Ding:** Writing – review & editing. **Xiaochen Chen:** Writing – review & editing. **Wenwen Chai:** Writing – review & editing. **Xu Cui:** Writing – review & editing. **Xiaolin Li:** Supervision, Writing – review & editing. **Deping Wang:** Supervision, Project administration, Funding acquisition. **Haobo Pan:** Supervision, Funding acquisition.

Declaration of competing interest

The authors declare that they have no competing interests.

Acknowledgments

Funding: This work was funded by National Key Research and

Development Program of China (Grant No. 2018YFC1106302 and 2018YFA0703100), National Natural Science Foundation of China (Grant No. 51772210, U2001221, 51802340, 81871774 and 82072422), Frontier Science Key Research Programs of CAS (Grant No. QYZDB-SSW-JSC030), and Shenzhen Fundamental Research Foundation (Grant No. JCYJ20200109114620793).

References

[1] NCCN Guidelines for patients: bone cancer. https://www.nccn.org/patients/guidelines/content/PDF/bone-patient.pdf, 2021, 2021.
[2] K. Weber, T.A. Damron, F.J. Frassica, F.H. Sim, Malignant bone tumors, Instr. Course Lect. 57 (2008) 673–688.
[3] T.T. Roberts, A.J. Rosenbaum, Bone grafts, bone substitutes and orthobiologics: the bridge between basic science and clinical advancements in fracture healing, Organogenesis 8 (2012) 114–124, https://doi.org/10.4161/org.23306.
[4] S.E.S. Leary, A.W. Wozniak, C.A. Billups, J. Wu, V. McPherson, M.D. Neel, B. N. Rao, N.C. Daw, Survival of pediatric patients after relapsed osteosarcoma: the st. Jude children's research hospital experience: relapsed osteosarcoma, Cancer 119 (2013) 2645–2653, https://doi.org/10.1002/cncr.28111.
[5] L. Polo-Corrales, M. Latorre-Esteves, J.E. Ramirez-Vick, Scaffold design for bone regeneration, J. Nanosci. Nanotechnol. 14 (2014) 15–56, https://doi.org/10.1166/jnn.2014.9127.
[6] J.R. Jones, L.M. Ehrenfried, L.L. Hench, Optimising bioactive glass scaffolds for bone tissue engineering, Biomaterials 27 (2006) 964–973, https://doi.org/10.1016/j.biomaterials.2005.07.017.
[7] T. Ghassemi, A. Shahroodi, M.H. Ebrahimzadeh, A. Mousavian, J. Movaffagh, A. Moradi, Current concepts in scaffolding for bone tissue engineering, Arch Bone Jt Surg 6 (2018) 90–99.
[8] D. Lin, Y. Chai, Y. Ma, B. Duan, Y. Yuan, C. Liu, Rapid Initiation of Guided Bone Regeneration Driven by Spatiotemporal Delivery of IL-8 and BMP-2 from Hierarchical MBG-Based Scaffold, Biomaterials, 2017, https://doi.org/10.1016/j.biomaterials.2017.11.011.
[9] S. Ramakrishna, Multifunctional bone scaffolds: from regeneration to bone cancer therapy, BJSTR 27 (2020) 21124–21128, https://doi.org/10.26717/BJSTR.2020.27.004572.
[10] W. Dang, T. Li, B. Li, H. Ma, D. Zhai, X. Wang, J. Chang, Y. Xiao, J. Wang, C. Wu, A bifunctional scaffold with CuFeSe2 nanocrystals for tumor therapy and bone reconstruction, Biomaterials 160 (2018) 92–106, https://doi.org/10.1016/j.biomaterials.2017.11.020.
[11] Y.L. Zhang, D. Zhai, M.C. Xu, Q.Q. Yao, J. Chang, C.T. Wu, 3D-printed bioceramic scaffolds with a Fe3O4/graphene oxide nanocomposite interface for hyperthermia therapy of bone tumor cells, J. Mater. Chem. B 4 (2016) 2874–2886, https://doi.org/10.1039/c6tb00390g.
[12] M. Hubert, A.J. Faber, On the structural role of boron in borosilicate glasses, Phys. Chem. Glasses 55 (2014) 136–158.
[13] M.N. Rahaman, D.E. Day, B.S. Bal, Q. Fu, S.B. Jung, L.F. Bonewald, A.P. Tomsia, Bioactive glass in tissue engineering, Acta Biomater. 7 (2011) 2355–2373, https://doi.org/10.1016/j.actbio.2011.03.016.
[14] G. Kaur, O.P. Pandey, K. Singh, D. Homa, B. Scott, G. Pickrell, A review of bioactive glasses: their structure, properties, fabrication and apatite formation, J. Biomed. Mater. Res. A. 102 (2014) 254–274, https://doi.org/10.1002/jbm.a.34690.
[15] D.S. Brauer, Bioactive glasses-structure and properties, Angew Chem. Int. Ed. Engl. 54 (2015) 4160–4181, https://doi.org/10.1002/anie.201405310.
[16] W. Liu, X. Dan, W.W. Lu, X. Zhao, C. Ruan, T. Wang, X. Cui, X. Zhai, Y. Ma, D. Wang, W. Huang, H. Pan, Spatial distribution of biomaterial microenvironment pH and its modulatory effect on osteoclasts at the early stage of bone defect regeneration, ACS Appl. Mater. Interfaces 11 (2019) 9557–9572.
[17] Y. Liu, R. Lin, L. Ma, H. Zhuang, C. Feng, J. Chang, C. Wu, Mesoporous bioactive glass for synergistic therapy of tumor and regeneration of bone tissue, Applied Materials Today 19 (2020) 100578, https://doi.org/10.1016/j.apmt.2020.100578.
[18] H. Zhuang, R. Lin, Y. Liu, M. Zhang, D. Zhai, Z. Huan, C. Wu, Three-dimensional-Printed bioceramic scaffolds with osteogenic activity for simultaneous photo/magnetothermal therapy of bone tumors, ACS Biomater. Sci. Eng. 5 (2019) 6725–6734.
[19] H. Wang, X. Zeng, L. Pang, H. Wang, B. Lin, Z. Deng, E.L.X. Qi, N. Miao, D. Wang, P. Huang, H. Hu, J. Li, Integrative treatment of anti-tumor/bone repair by combination of MoS2 nanosheets with 3D printed bioactive borosilicate glass scaffolds, Chem. Eng. J. 396 (2020) 125081, https://doi.org/10.1016/j.cej.2020.125081.
[20] M. Strli, A comparative study of several transition metals in Fenton-like reaction systems at circum-neutral pH, Acta Chim. Slov. (2003) 619–632.
[21] B. Lin, H. Chen, D. Liang, W. Lin, X. Qi, H. Liu, X. Deng, Acidic pH and high-H2O2 dual tumor microenvironment-responsive nanocatalytic graphene oxide for cancer selective therapy and recognition, ACS Appl. Mater. Interfaces 11 (2019) 11157–11166, https://doi.org/10.1021/acsami.8b22487.
[22] Z. Tang, Y. Liu, M. He, W. Bu, Chemodynamic therapy: tumour microenvironment-mediated Fenton and fenton-like reactions, Angew Chem. Int. Ed. Engl. 58 (2019) 946–956, https://doi.org/10.1002/anie.201805664.
[23] S.-Y. Yin, G. Song, Y. Yang, Y. Zhao, P. Wang, L.-M. Zhu, X. Yin, X.-B. Zhang, Persistent regulation of tumor microenvironment via circulating catalysis of MnFe2O4 @Metal–Organic frameworks for enhanced photodynamic therapy, Adv. Funct. Mater. (2019) 1901417, https://doi.org/10.1002/adfm.201901417.
[24] B. Ma, S. Wang, F. Liu, S. Zhang, J. Duan, Z. Li, Y. Kong, Y. Sang, H. Liu, W. Bu, L. Li, Self-assembled copper-amino acid nanoparticles for in situ glutathione "AND" H2O2 sequentially triggered chemodynamic therapy, J. Am. Chem. Soc. 141 (2019) 849–857, https://doi.org/10.1021/jacs.8b08714.
[25] B. Yang, Y. Chen, J. Shi, Reactive oxygen species (ROS)-based nanomedicine, Chem. Rev. 119 (2019) 4881–4985, https://doi.org/10.1021/acs.chemrev.8b00626.
[26] C. Zhang, W. Bu, D. Ni, S. Zhang, Q. Li, Z. Yao, J. Zhang, H. Yao, Z. Wang, J. Shi, Synthesis of iron nanometallic glasses and their application in cancer therapy by a localized Fenton reaction, Angew Chem. Int. Ed. Engl. 55 (2016) 2101–2106, https://doi.org/10.1002/anie.201510031.
[27] K. Glenske, P. Donkiewicz, A. Köwitsch, N. Milosevic-Oljaca, P. Rider, S. Rofall, J. Franke, O. Jung, R. Smeets, R. Schnettler, S. Wenisch, M. Barbeck, Applications of metals for bone regeneration, Int. J. Math. Stat. 19 (2018) 826, https://doi.org/10.3390/ijms19030826.
[28] H. Wang, S. Zhao, J. Zhou, Y. Shen, W. Huang, C. Zhang, M.N. Rahaman, D. Wang, Evaluation of borate bioactive glass scaffolds as a controlled delivery system for copper ions in stimulating osteogenesis and angiogenesis in bone healing, J. Mater. Chem. B. 2 (2014) 8547–8557, https://doi.org/10.1039/c4tb01355g.
[29] K. Zheng, A.R. Boccaccini, Sol-gel processing of bioactive glass nanoparticles: a review, Adv. Colloid Interface Sci. 249 (2017) 363–373, https://doi.org/10.1016/j.cis.2017.03.008.
[30] M. Shi, Z. Chen, S. Farnaghi, T. Friis, X. Mao, Y. Xiao, C. Wu, Copper-doped mesoporous silica nanospheres, a promising immunomodulatory agent for inducing osteogenesis, Acta Biomater. 30 (2016) 334–344, https://doi.org/10.1016/j.actbio.2015.11.033.
[31] L. Pang, Y. Shen, H. Hu, X. Zeng, W. Huang, H. Gao, H. Wang, D. Wang, Chemically and physically cross-linked polyvinyl alcohol-borosilicate gel hybrid scaffolds for bone regeneration, Mater. Sci. Eng. C 105 (2019) 110076, https://doi.org/10.1016/j.msec.2019.110076.
[32] H. Hu, Y. Tang, L. Pang, C. Lin, W. Huang, D. Wang, W. Jia, Angiogenesis and full-thickness wound healing efficiency of a copper-doped borate bioactive glass/poly (lactic-co-glycolic acid) dressing loaded with vitamin E in vivo and in vitro, ACS Appl. Mater. Interfaces 10 (2018) 22939–22950, https://doi.org/10.1021/acsami.8b04903.
[33] Q. Jia, J. Ge, W. Liu, X. Zheng, S. Chen, Y. Wen, H. Zhang, P. Wang, A magnetofluorescent carbon dot assembly as an acidic H2 O2 -driven oxygenerator to regulate tumor hypoxia for simultaneous bimodal imaging and enhanced photodynamic therapy, Adv. Mater. 30 (2018), e1706090, https://doi.org/10.1002/adma.201706090.
[34] C. Luo, J. Sun, D. Liu, B. Sun, L. Miao, S. Musetti, J. Li, X. Han, Y. Du, L. Li, L. Huang, Z. He, Self-assembled redox dual-responsive prodrug-nanosystem formed by single thioether-bridged paclitaxel-fatty acid conjugate for cancer chemotherapy, Nano Lett. 16 (2016) 5401–5408, https://doi.org/10.1021/acs.nanolett.6b01632.
[35] T. Kobayashi, M. Kato-Itoh, H. Nakauchi, Targeted organ generation using Mixl1-inducible mouse pluripotent stem cells in blastocyst complementation, Stem Cell. Dev. 24 (2015) 182–189.
[36] G. Shao, X. Wu, Y. Kong, S. Cui, X. Shen, C. Jiao, J. Jiao, Thermal shock behavior and infrared radiation property of integrative insulations consisting of MoSi2/borosilicate glass coating and fibrous ZrO2 ceramic substrate, Surf. Coating. Technol. 270 (2015) 154–163, https://doi.org/10.1016/j.surfcoat.2015.03.008.
[37] E.S. Ilton, J.E. Post, P.J. Heaney, F.T. Ling, S.N. Kerisit, XPS determination of Mn oxidation states in Mn (hydr)oxides, Appl. Surf. Sci. 366 (2016) 475–485, https://doi.org/10.1016/j.apsusc.2015.12.159.
[38] B.H.D. Son, V.Q. Mai, D.X. Du, N.H. Phong, N.D. Cuong, D.Q. Khieu, Catalytic wet peroxide oxidation of phenol solution over Fe–Mn binary oxides diatomite composite, J. Porous Mater. 24 (2016) 601–611, https://doi.org/10.1007/s10934-016-0296-7.
[39] H. Wang, S. Zhao, W. Xiao, J. Xue, Y. Shen, J. Zhou, W. Huang, M.N. Rahaman, C. Zhang, D. Wang, Influence of Cu doping in borosilicate bioactive glass and the properties of its derived scaffolds, Mater. Sci. Eng. C Mater. Biol. Appl. 58 (2016) 194–203, https://doi.org/10.1016/j.msec.2015.08.027.
[40] B.R. Barrioni, P. Naruphontjirakul, E. Norris, S. Li, N.L. Kelly, J.V. Hanna, M. M. Stevens, J.R. Jones, M. de M. Pereira, Effects of manganese incorporation on the morphology, structure and cytotoxicity of spherical bioactive glass nanoparticles, J. Colloid Interface Sci. 547 (2019) 382–392.
[41] I. Cacciotti, Bivalent cationic ions doped bioactive glasses: the influence of magnesium, zinc, strontium and copper on the physical and biological properties, J. Mater. Sci. 52 (2017) 8812–8831.
[42] T. Wu, H. Shi, Y. Liang, T. Lu, Z. Lin, J. Ye, Improving osteogenesis of calcium phosphate bone cement by incorporating with manganese doped β-tricalcium phosphate, Mater. Sci. Eng. C 109 (2020) 110481.
[43] L. Weng, S.K. Boda, M.J. Teusink, F.D. Shuler, X. Li, J. Xie, Binary doping of strontium and copper enhancing osteogenesis and angiogenesis of bioactive glass nanofibers while suppressing osteoclast activity, ACS Appl. Mater. Interfaces 9 (2017) 24484–24496.
[44] Y.S. Jung, W.T. Lim, J. Park, Y. Kim, Effect of pH on Fenton and fenton-like oxidation, Environ. Technol. 30 (2009) 183–190, https://doi.org/10.1080/09593330802468848.
[45] S. Jarvis, E. Koumadoraki, N. Madouros, S. Sharif, A. Saleem, S. Khan, Non-rodent animal models of osteosarcoma: a review, Cancer Treatment and Research Communications 27 (2021) 100307, https://doi.org/10.1016/j.ctarc.2021.100307.
[46] X. Cui, Y. Zhang, J. Wang, C. Huang, Y. Wang, H. Yang, W. Liu, T. Wang, D. Wang, G. Wang, C. Ruan, D. Chen, W.W. Lu, W. Huang, M.N. Rahaman, H. Pan, Strontium

modulates osteogenic activity of bone cement composed of bioactive borosilicate glass particles by activating Wnt/β-catenin signaling pathway, Bioactive Materials 5 (2020) 334–347.

[47] W. Liu, T. Wang, C. Yang, B.W. Darvell, J. Wu, K. Lin, J. Chang, H. Pan, W.W. Lu, Alkaline biodegradable implants for osteoporotic bone defects—importance of microenvironment pH, Osteoporos. Int. 27 (2016) 93–104.

[48] V. Schirrmacher, From chemotherapy to biological therapy: a review of novel concepts to reduce the side effects of systemic cancer treatment (Review), Int. J. Oncol. 54 (2019) 407–419.

[49] X. Wang, X. Zhong, Z. Liu, L. Cheng, Recent progress of chemodynamic therapy-induced combination cancer therapy, Nano Today 35 (2020) 100946, https://doi.org/10.1016/j.nantod.2020.100946.